A Study of the Deformation of Patented Steel Wire

GEORGE LANGFORD

Comparisons of transmission electron micrographs of transverse sections of heavily drawn patented steel wire with existing metallographic and strength data were made with the aid of a computer. Both fragmentation of the cementite and the local deformation mode within the wire, *i.e.*, plane strain elongation, an effect of the ⟨110⟩ wire texture of the ferrite, were taken into account in order to obtain a model for large-strain deformation of pearlitic or bainitic microstructures which is consistent with the observed microstructural changes and strain hardening rate. The functional dependence of this model on true strain and original substructural spacing is similar to the equation of Embury and Fisher for the strain hardening of drawn pearlite because their assumptions (no fragmentation of the cementite and homogeneous, axially symmetric elongation) produced offsetting errors. The present model allows for additional sensitivity of the strain hardening rate of drawn patented steel wire to metallurgical and processing variables over and above the simple dependence on original substructural scale predicted by the model of Embury and Fisher.

DRAWN patented carbon steel wire has a fibrous microstructure when viewed in a longitudinal cross section with the electron microscope[1,2] but a "wavy" microstructure when viewed in a transverse cross section.[3,4]

Embury and Fisher[1] found, from their measurements on longitudinal sections, a direct proportionality between the characteristic transverse dimension of this substructure and the diameter of the as-drawn wire. This seemed to indicate that the carbide particles or lamellae completely inhibited dynamic recovery. They therefore proposed an equation which accounted simply for the observed strength-prior strain relation of these wires:

$$\sigma = \sigma_0 + \frac{k_y}{\sqrt{2d_0}} \exp(\epsilon/4) \qquad [1]$$

where σ_0 is the "lattice friction" stress, d_0 is the original substructural spacing, k_y is the Hall-Petch proportionality constant, ϵ is the true wire-drawing strain,* and σ is the resultant flow stress of the material. This relation, with strength proportional to $\exp(\epsilon/4)$, seems to be a limiting case, since the data of Chandhok *et al.*[2] for patented steel wire drawn at various temperatures above and below room temperature approached this behavior more closely, the lower the deformation temperature. For convenience, these data are replotted in Fig. 1.

*True stresses and strains are used throughout this paper. The strains are given by the well-known expression, 2 in (D_0/D), where D_0 and D are the original and instantaneous specimen diameters, respectively.

On the other hand, transverse sections of similar material, as shown in the micrographs of Dewey and Briers[3] and Glenn *et al.*[4] as well as in this paper, exhibit the characteristic "wavy" or "curly-grain" microstructure known, at least in single-phase materials, to be associated with the ⟨110⟩ bcc wire texture.[5-8] This implies that the local shape change is plane strain, as explained by Hosford.[7] It should be mentioned that patented steel wires also are known to have a ⟨110⟩ wire texture.[9]

If the local shape change corresponds to plane strain, then the interlamellar spacing of pearlite oriented parallel to the wire axis and perpendicular to the most rapidly changing transverse dimension of a microregion* should be inversely proportional to the wire length and, therefore, proportional to the square of the wire diameter, if no dynamic recovery occurs. The latter relationship has been observed by Glenn *et al.*[4] in the same drawn patented steel wire used in this study, where the finest resolvable inter-

*In this paper the term, "microregion", is used to describe one of the units or swirls in the wavy microstructure of a transverse section of the drawn pearlite. Each microregion corresponds approximately to a pearlite colony or at least part of that colony. Viewed in three dimensions each microregion is ribbon-shaped, with the long dimension straight and parallel to the wire axis.

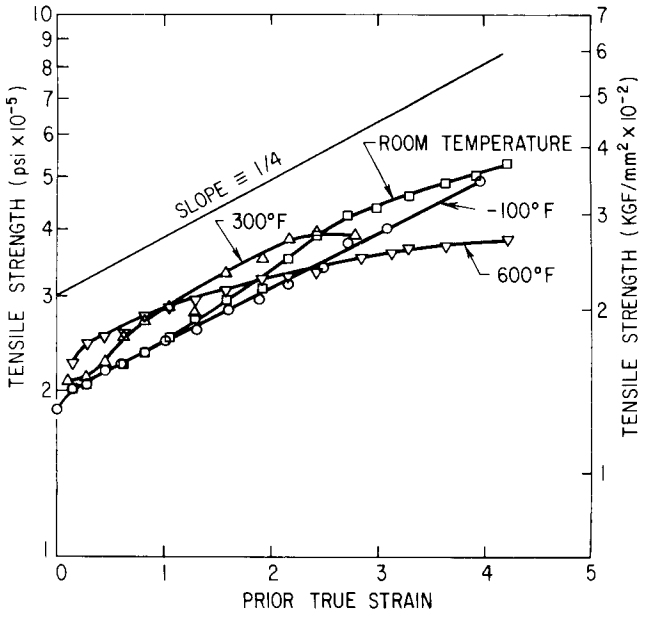

Fig. 1—Room-temperature tensile strengths of patented steel wires as a function of prior strain at various temperatures, after Chandhok *et al.*[2]

GEORGE LANGFORD is Scientist, E. C. Bain Laboratory for Fundamental Research, U. S. Steel Corporation, Monroeville, Pa.

Manuscript submitted May 21, 1969.

lamellar spacing measured on transmission electron micrographs of transverse sections of the drawn wires was plotted as a function of the square of the wire diameter.

The present work was undertaken because these separate observations on longitudinal and transverse sections seem to be incompatible. If the local shape change is indeed plane strain elongation, then either a Hall-Petch relation (strength proportional to (interlamellar spacing)$^{-1/2}$) is not followed, or the actual strength-controlling intercept is not the extrapolated interlamellar spacing, implying that some kind of dynamic recovery is taking place. Due to the absence of any information leading to such a weak strengthening effect of the intercept size (such as, strength proportional to (interlamellar spacing)$^{-1/4}$) it will be assumed in the rest of this paper that a Hall-Petch relation is the correct one to be used here.

By a detailed calculation of the change in shape of microregions and of the change in pearlite spacings with strain, the effects of various assumptions regarding the local mode of deformation upon the calculated strength-strain relationship and microstructural changes can be investigated. These potential models must predict 1) the experimentally observed changes of the flow stress and 2) the characteristic changes of scale and shape of the microstructure brought about by the wire-drawing deformation.

Table I. Chemical Composition of Steel Used in This Study

Element	Composition, percent
C	0.94
Mn	0.43
P	0.006
S	0.002
Si	0.065
Cu	0.005
Ni	0.004
Cr	0.050
Mo	<0.005
V	0.005
Ti	<0.005
N	0.002
Acid Sol Al	0.043
O	12 ppm
Sn	<0.001

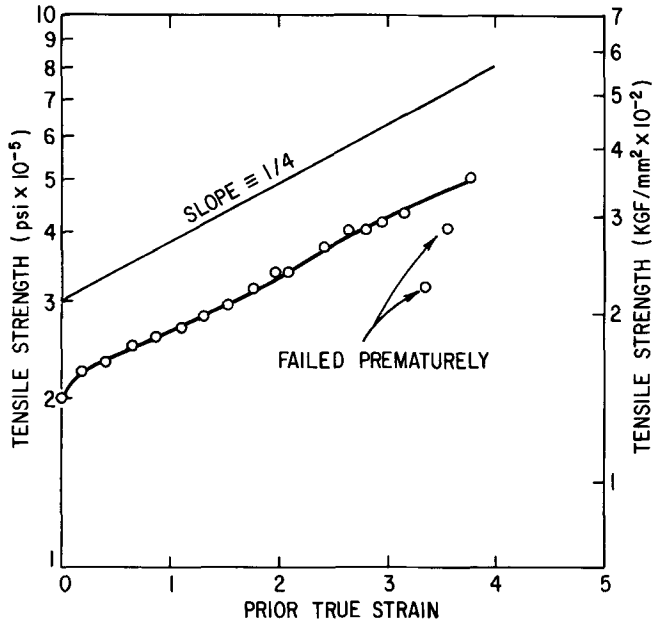

Fig. 2—Tensile strengths of the patented steel wire used for the transmission electron micrographs in this paper, as a function of prior strain, after Spare *et al.*[10]

EXPERIMENTAL

A series of samples drawn from a 0.220 in. (5.60 mm) diam patented steel wire were provided by G. T. Spare of the Applied Research Laboratory. The chemical analysis is shown in Table I and the previously determined tensile strengths of the wires[10] are replotted according to the convention used in this paper in Fig. 2.

Transverse discs 0.015 in. (0.38 mm) thick were cut from the wires on a Servomet spark-discharge machine, modified by the wire electrode shown in Fig. 3. These discs were subsequently wet ground on abrasive paper to about 0.001 in. (0.025 mm) and electrolytically thinned by the technique of Glenn and Schoone.[11] Transmission electron micrographs were made of the resultant thin foils. This is also the series from which Fig. 4 of Ref. 4 was prepared.

Fig. 4 of this paper shows the development of the characteristic "wavy" microstructure as a function of

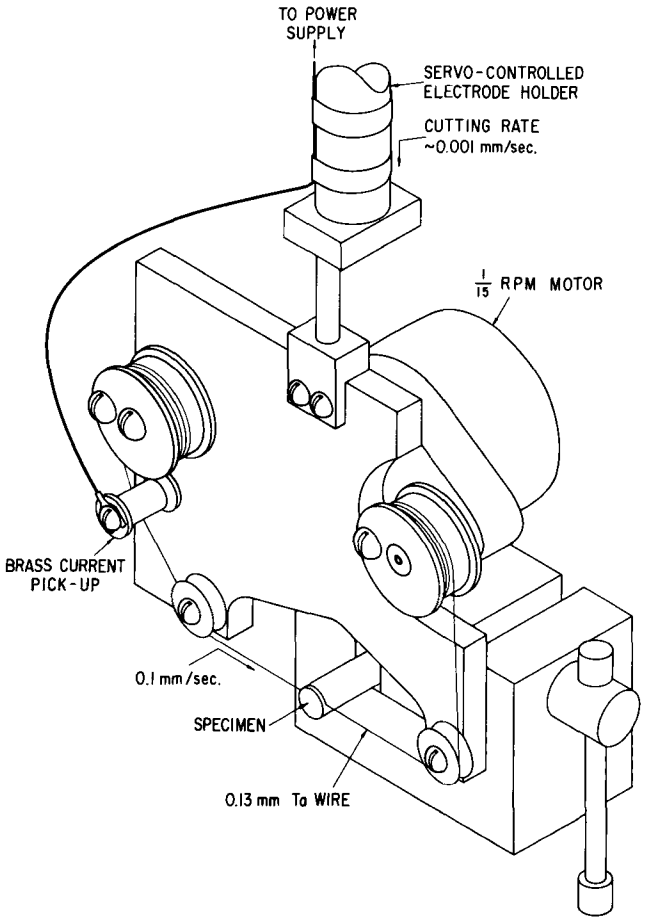

Fig. 3—Schematic representation of wire electrode used in spark-cutting transverse sections for transmission electron microscopy.

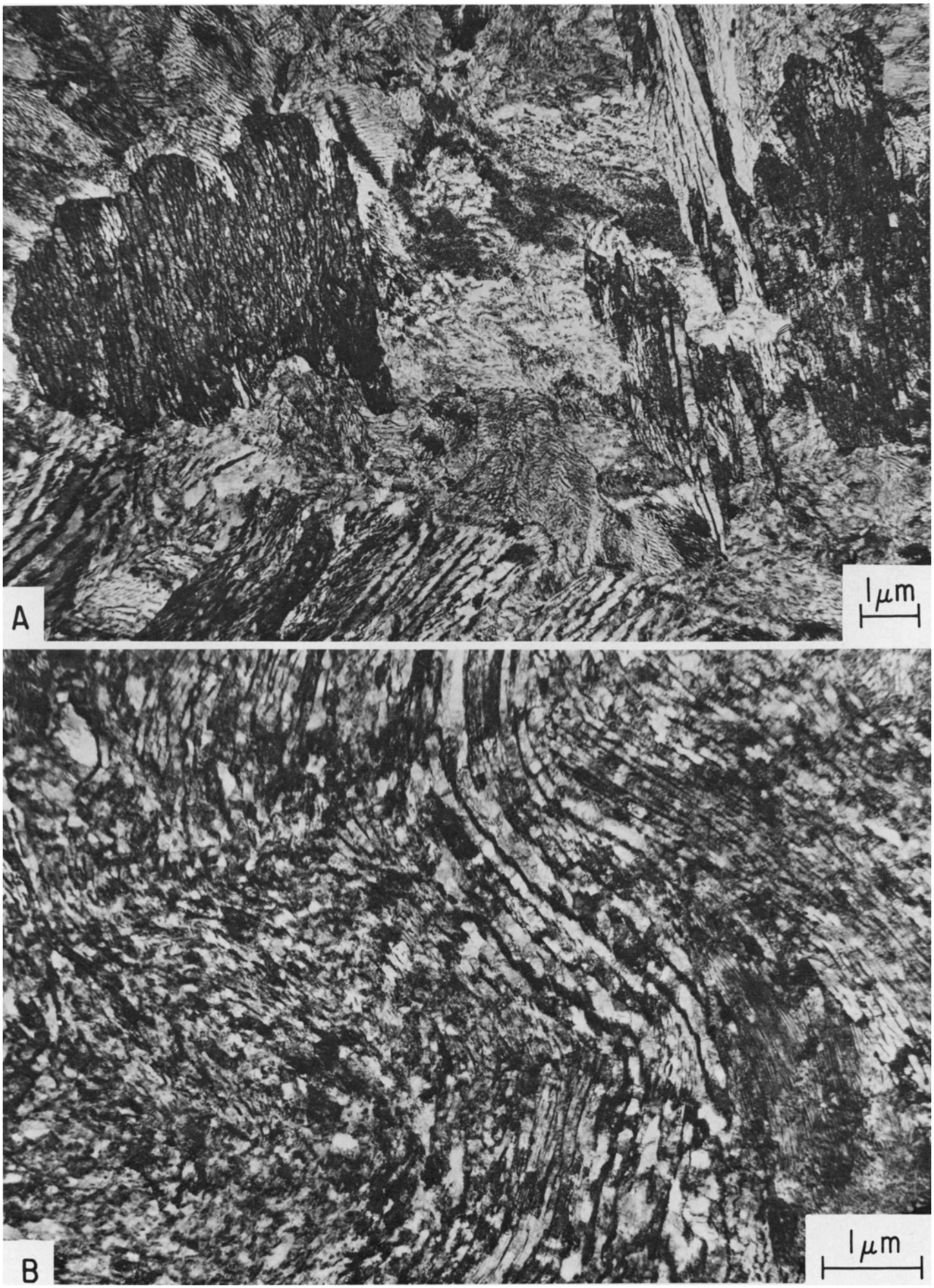

Fig. 4—Transmission electron micrographs of transverse sections of drawn patented steel wire as a function of prior strain, ϵ. (*a*) $\epsilon = 0$, (*b*) $\epsilon = 1.1$, (*c*) $\epsilon = 2.0$, (*d*) $\epsilon = 2.6$, (*e*) $\epsilon = 3.2$, (*f*) $\epsilon = 3.8$.

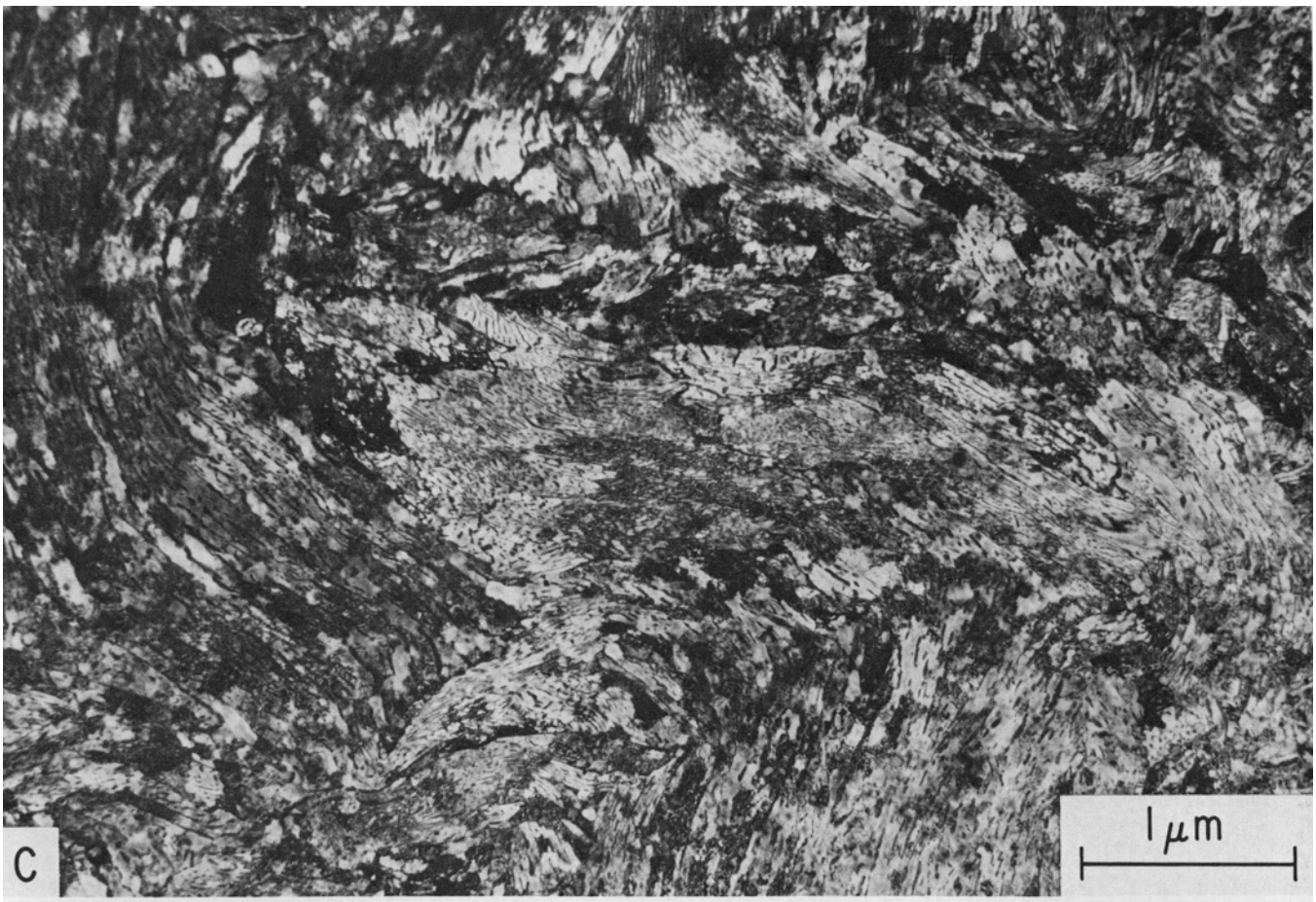

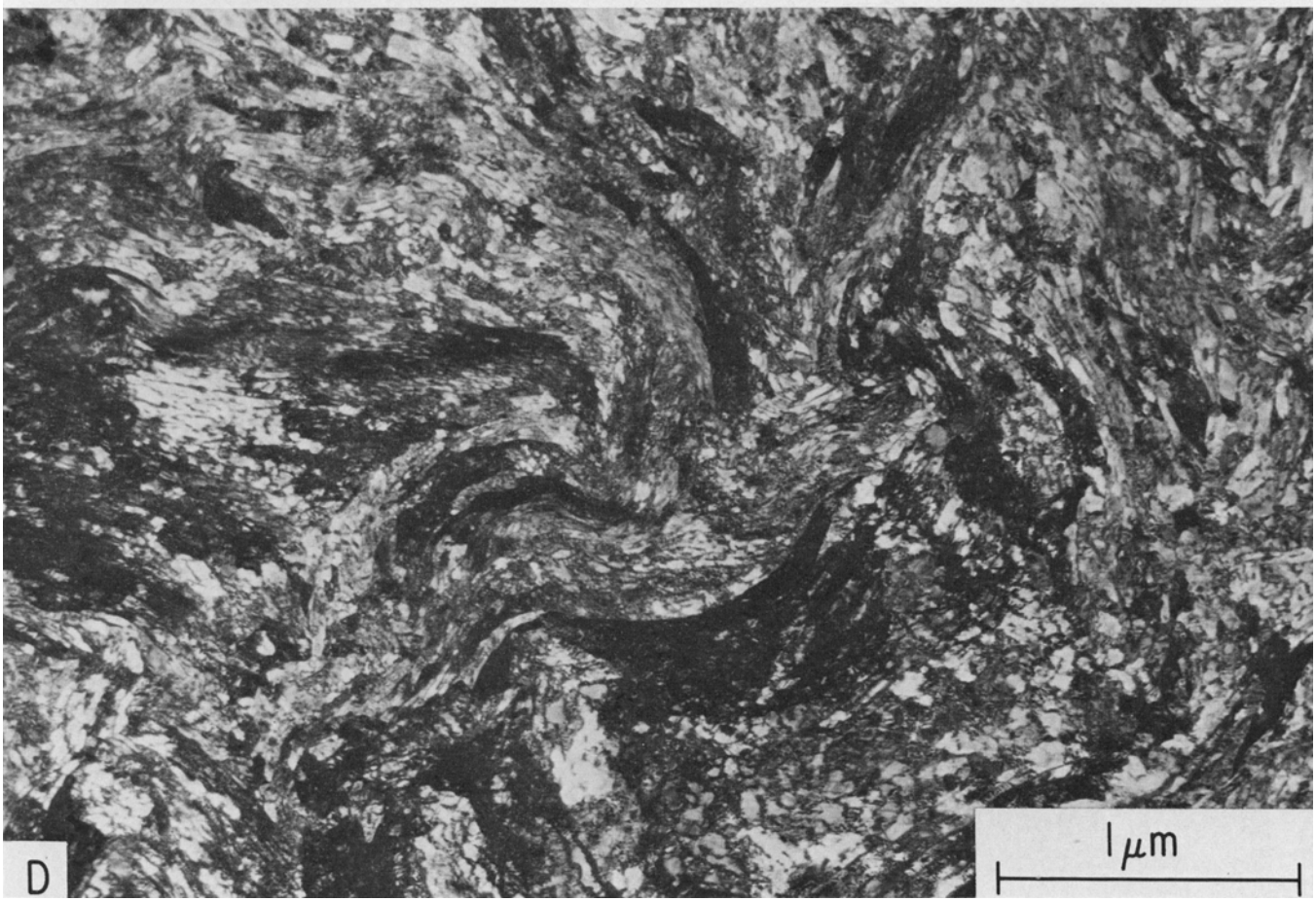

Fig. 4 (Continued)

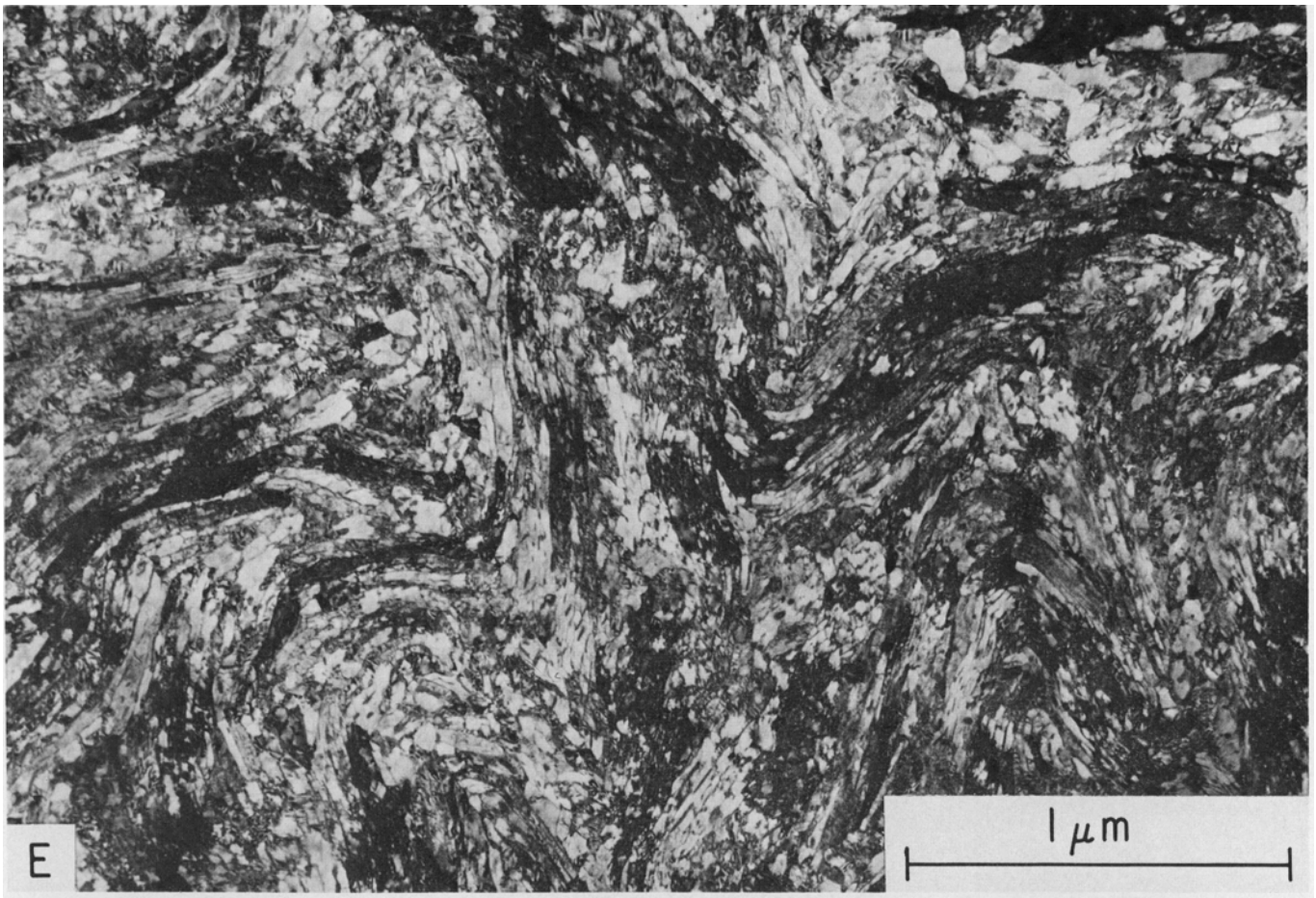

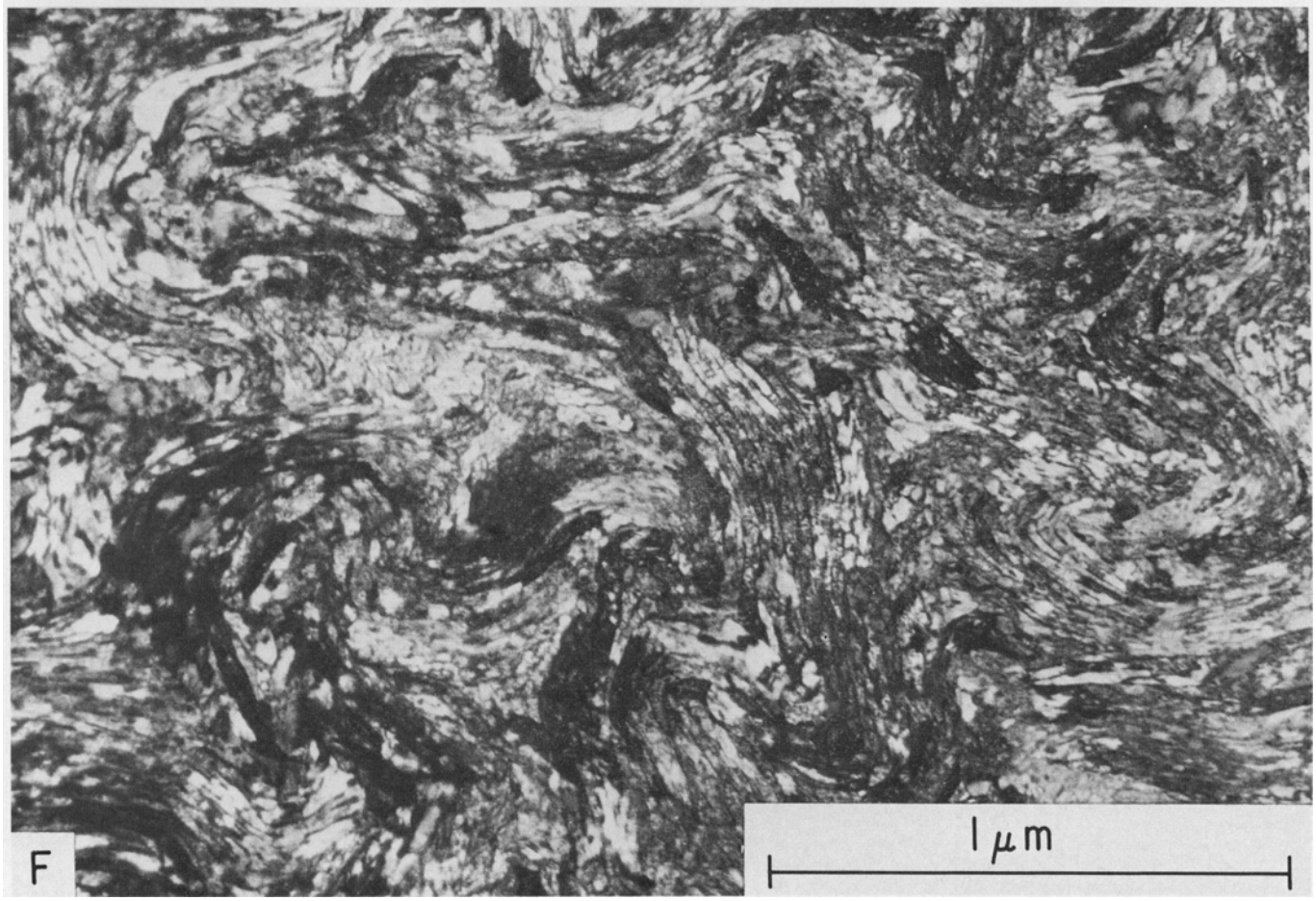

Fig. 4 (Continued)

wire-drawing strain. The micrographs are enlarged by a progressively greater factor to compensate for the decreasing wire diameter, in order to aid the observation of the microstructural shape change. There appears to be no orientation relationship between the thin direction of a ribbonlike microregion and the orientation of the pearlite lamellae within it. Two extremes of this behavior are shown in Fig. 5. In one area of the micrograph, a, the pearlite lamellae are apparently perpendicular to the direction of thinning (parallel to the thin dimension of a microregion) whereas in area b the lamellae are parallel to the direction of thinning. In the former case the apparent pearlite spacing is smaller than would be predicted by simple proportionality to the wire diameter, while in the latter case the apparent spacing is larger than would be so predicted. There are many more examples of case a than case b.

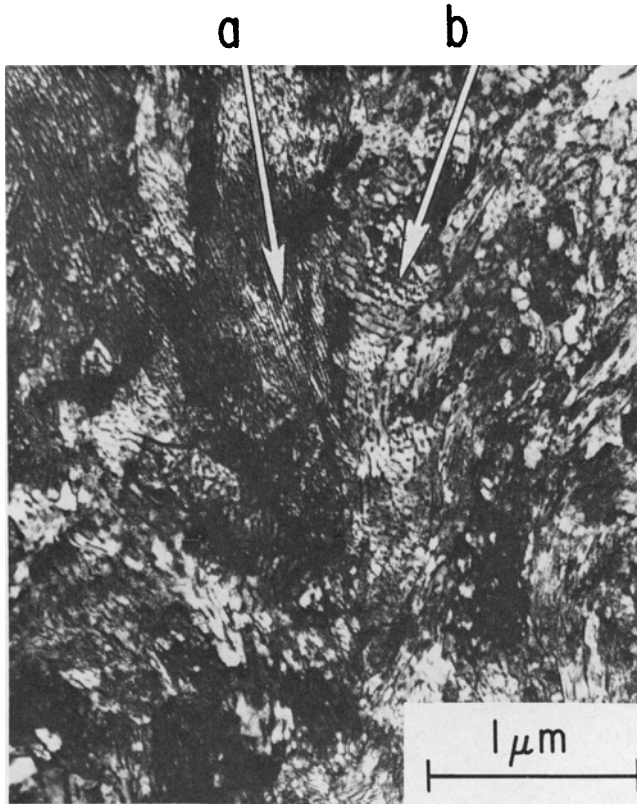

Fig. 5—Transmission electron micrograph of a transverse section of a patented steel wire drawn to a strain of 2.0, showing two extremes of the orientation relationship between a ribbonlike microregion and the pearlite lamellae.

Fig. 6—Transmission electron micrograph of upper bainite in as-patented steel wire.

Only a fraction of the as-patented structure of this steel consists of recognizable classically lamellar pearlite; the balance is either upper bainite or pearlite unfavorably oriented with respect to the foil. The 950°F (510°C) transformation temperature favors the formation of both microconstituents. The appearance of the bainite is much like a fragmented pearlite; that is, the cementite "lamellae" actually consist of rows or sheets of fine platelets, Fig. 6. Because of the resulting uncertainty about the original appearance of a given region in the drawn wire, it is difficult to discuss the integrity of the cementite lamellae following wire-drawing. It is only possible to say that *some* of the pearlite is deformed without fragmentation of the cementite, Fig. 7, but that there is less recognizably perfect pearlite in the microstructures of the drawn wires than in the undrawn wires. None of the voids previously reported[12] between the ends of fractured cementite lamellae in bent drawn or undrawn wires of coarse pearlite were observed here in transverse sections of drawn wires.

MODELS AND COMPUTER CALCULATIONS

A model for the deformation of pearlite must be consistent with the experimental observations on drawn patented steel wires, which are summarized below:

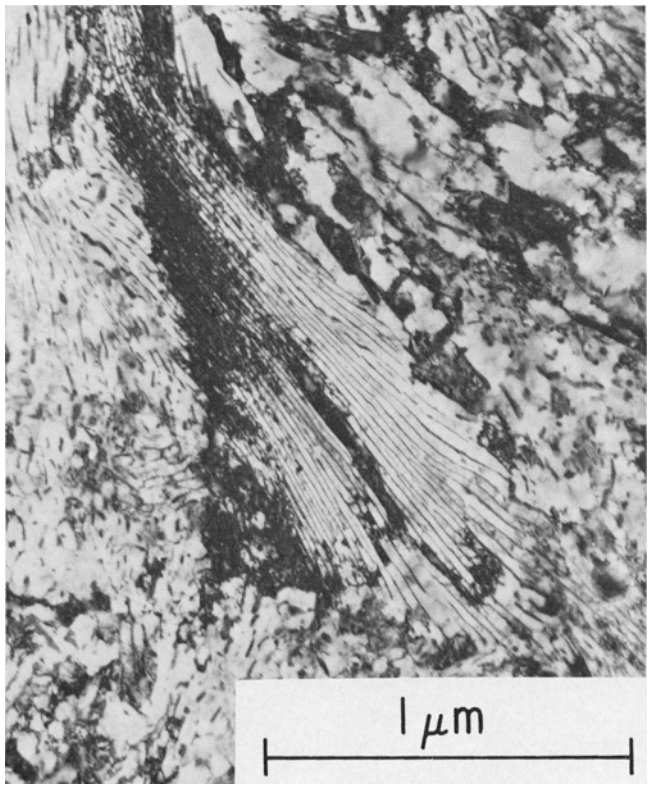

Fig. 7—Transmission electron micrograph of a transverse section of the neck of a tensile specimen of drawn patented steel wire showing heavily deformed but intact pearlite, ϵ = 0.7(drawing) + 0.7(necking) = 1.4 total.

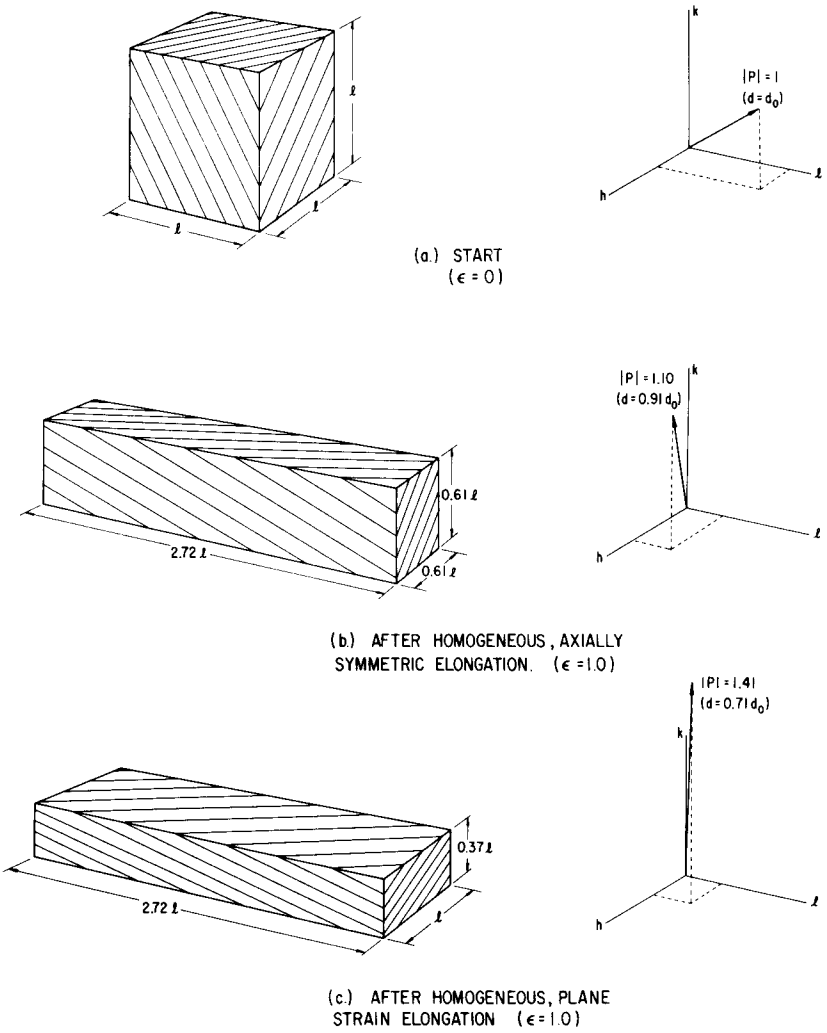

Fig. 8—Schematic representation of the changes of interlamellar spacing and orientation brought about by homogeneous elongation.

1) The rate of strain hardening, when plotted as $\ln(\sigma - \sigma_0)$ vs ϵ, has a slope of $\frac{1}{4}$.

2) A "wavy" structure develops in a transverse section and becomes more apparent, the greater the strain.

3) The range of apparent pearlite spacings broadens with increasing strain.

The following discussion contains the quantitative evaluation of the behavior of a series of potential models and combinations of models during hypothetical wire-drawing deformation.

Three modes of deformation are considered: 1) homogeneous axially symmetric elongation, 2) homogeneous plane strain elongation, and 3) inhomogeneous intralamellar shear, producing inhomogeneous plane strain elongation. Mode 1) would be expected in an isotropic continuum. Mode 2) is considered to be an effect of the ⟨110⟩ bcc wire texture; the intercurling of the ribbon-like microregions to maintain constant aggregate volume is not considered in order to simplify the calculations. Mode 3) is considered in combination with each of the other modes in order to take account of a second potential mechanism of formation of the wavy microstructure. The question of the integrity of the cementite is also taken into account.

In the following discussion the usual terms used to describe pearlite, lamellae, colonies, and so forth, will be used in like manner to describe the hypothetical model.

COMPUTATION METHOD

During homogeneous deformation by axisymmetric elongation or plane strain elongation the transverse dimensions of a finite medium are reduced, while its length is increased. As shown in Fig. 8 this should have the effect of changing the spacing of an isotropic lamellar aggregate and geometrically rotating the lamellae towards parallelism with the tensile axis (for axially symmetric elongation) or with the plane of the ribbon (for plane strain elongation). At infinite elongation, all lamellae will be completely reoriented and will have zero spacing, even without lamellar reorientation by nonhomogeneous flow.

The spacing of the ith pearlite colony, a region where the pearlite is of the same orientation and spacing, is:

$$d_i = d_0/\sqrt{h_i^2 + k_i^2 + l_i^2} \qquad [2]$$

where d_0 is the original interlamellar spacing of all the colonies, and h_i, k_i, l_i are the coordinates of a vector P_i which is perpendicular to the lamellae and whose magnitude is the ratio of original to instantaneous spacing at a given strain. These coordinates vary

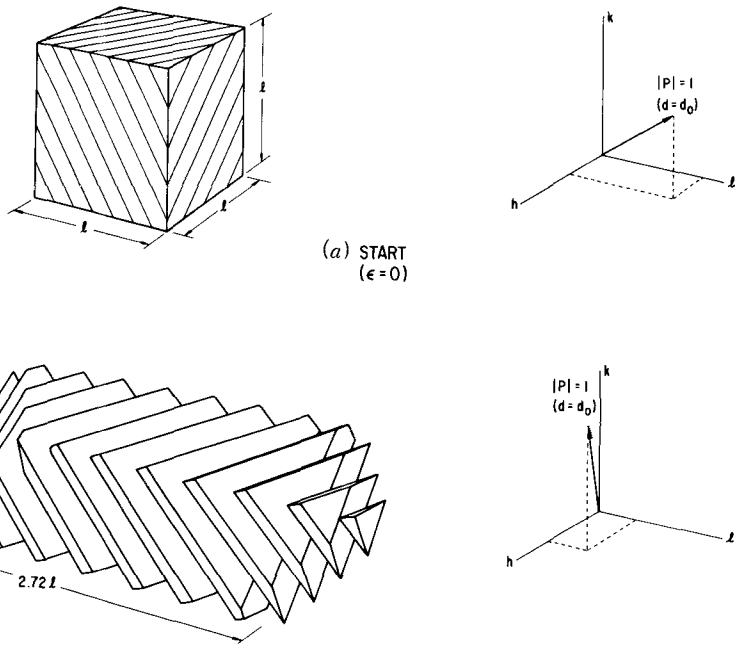

Fig. 9—Schematic representation of the process of elongation by inhomogeneous intralamellar shear (deck-of-cards deformation) indicating the change of orientation and the effectively plane strain elongation without a change in the interlamellar spacing.

with strain (ϵ) according to the following equations:

$$h_i = h_i^\circ f_1(\epsilon) \quad [3]$$

$$k_i = k_i^\circ f_2(\epsilon) \quad [4]$$

$$l_i = l_i^\circ f_3(\epsilon) \quad [5]$$

where f_1, f_2, and f_3 are different functions of strain depending on the type of deformation, and h_i°, k_i°, l_i° are the coordinates of the original vector P_i°.

By reference to Fig. 8 it can be seen that the coordinates (h_i, k_i, l_i) of the vector P_i vary inversely with the changes in dimensions of the aggregate, so that for axially symmetric elongation, assuming constant volume,

$$f_1(\epsilon) = \exp(\epsilon/2) \quad [6]$$

$$f_2(\epsilon) = \exp(\epsilon/2) \quad [7]$$

$$f_3(\epsilon) = \exp(-\epsilon) \quad [8]$$

For plane strain elongation,

$$f_1(\epsilon) = \exp(\epsilon) \quad [9]$$

$$f_2(\epsilon) = 1 \quad [10]$$

$$f_3(\epsilon) = \exp(-\epsilon) \quad [11]$$

When all the colonies have the same initial spacing, the loci of the tips of the vectors P_i will form a sphere; if the lamellae are randomly oriented, the distribution of the vector tips will be uniform over the surface of that sphere:*

*In the computer program, the vectors (P_i) are drawn to the centers of equal-sized "rectangles", bounded by continuous lines of latitude and discontinuous lines of longitude, drawn on the surface of an octant of a sphere. The surface has the appearance of the wall of an Eskimo igloo.

$$(h_i^\circ)^2 + (k_i^\circ)^2 + (l_i^\circ)^2 = 1 \quad [12]$$

In the case where the aggregate is weaker in the lamellar plane, there is also the possibility of nonhomogeneous deformation by shear within and parallel to the lamellae, similar to the sliding of a deck of of cards, as shown in Fig. 9. If the slip direction is in the same direction as the maximum shear stress on that plane, the plane of the ensuing plane strain intersects the long axis of the aggregate as also shown in Fig. 9. In this case there is no change in the lamellar spacing as all the shear displacement would be confined to the plane of the lamellae; the aggregate is assumed to be free to rotate to accommodate the resultant rotation. This means that:

$$(h_i)^2 + (k_i)^2 + (l_i)^2 = (h_i^\circ)^2 + (k_i^\circ)^2 + (l_i^\circ)^2 \quad [13]$$

With reference to Fig. 9, the corresponding equations for the components of the vectors (P_i) are:

$$h_i = \left[\{[(h_i^\circ)^2 + (k_i^\circ)^2 + (l_i^\circ)^2] - (l_i^\circ)^2 \exp(-2\epsilon)\}\left\{\frac{(h_i^\circ)^2}{(h_i^\circ)^2 + (k_i^\circ)^2}\right\}\right]^{1/2} \quad [14]$$

$$k_i = \left(\frac{k_i^\circ}{h_i^\circ}\right)h_i \quad [15]$$

If $h_i^\circ = 0$, then

$$k_i = \{(k_i^\circ)^2 + (l_i^\circ)^2[1 - \exp(-2\epsilon)]\}^{1/2} \quad [15a]$$

In either case,

$$l_i = l_i^\circ \exp(-\epsilon) \quad [16]$$

The shear stress resolved in the plane of the lamellae is

$$\tau_{res}^i = \frac{\sigma_{hom}^i}{2} \sin 2\phi_i \quad [17]$$

where (σ_{hom}^i) is the stress for homogeneous flow of that colony and ϕ_i is the angle between the tensile

axis and the vector P_i. Nonhomogeneous flow occurs under a stress (σ^i_{nhom}) when τ^i_{res} reaches a critical value, τ_c:

$$\sigma^i_{\text{nhom}} = \frac{2\tau_c}{\sin 2\phi_i} \quad [18]$$

τ_c is assumed to be a fraction α ($0 < \alpha < 1$) of the shear stress for homogeneous flow of the aggregate. Thus

$$\sigma^i_{\text{flow}} = \frac{2(\alpha\sigma^i_{\text{hom}}/2)}{\sin 2\phi_i} = \left(\frac{\alpha}{\sin 2\phi_i}\right)\sigma^i_{\text{hom}} \quad [19]$$

The stress for homogeneous deformation (σ^i_{hom}) is assumed to be related to the linear-intercept interlamellar spacing in the direction of maximum shear stress. This relationship is assumed to be

$$\sigma^i_{\text{hom}} = \sigma_0 + k_y(\bar{d}_i)^{-1/2} \quad [20]$$

which is the well-known Hall-Petch relation as first applied to the problem of the deformation of pearlite by Embury and Fisher.[1] In this calculation, k_y, σ_0, and d_0 were chosen so as to obtain the same initial strength as patented pearlite. If ($\alpha/\sin 2\phi_i$) is less than unity, deformation is considered to take place by the deck-of-cards mechanism, with the flow stress of the ith colony given by Eq. [19], but if ($\alpha/\sin 2\phi_i$) is greater than unity, homogeneous deformation takes place under the stress given by Eq. [20]. Since the aggregate is by definition of the problem fully plastic, however, there will be a finite strain rate by one deformation mode superimposed on the other at all times. For simplicity, this effect is not taken into account in the calculations; it will be seen later that this is justified for the present problem.

In the strength calculations, $\bar{d}_i$ was taken as the mean linear interlamellar intercept in the direction of maximum shear stress, which is at a 45 deg angle to the longitudinal axis. There is a slight dependence of $\bar{d}_i$ on the orientation of the pearlite colony. For purposes of comparison with actual measurements the apparent spacings on a transverse section of the hypothetical aggregate have also been calculated.

Each hypothetical pearlite colony will therefore have a unique stress-strain relationship dependent on its original orientation; the stress-strain curve for the aggregate is the average of all the colonies. Since an analytical average requires an elliptic integral, the computation was done for a finite number of colonies by first determining the strain limits of the deck-of-cards deformation mode for each colony and then computing the average strength of the aggregate from the strength of each colony, at each increment of strain.

PRESENTATION AND DISCUSSION OF COMPUTER RESULTS

Fig. 10 contains a family of flow stress-strain curves calculated for various combinations of homogeneous axially symmetric elongation and inhomogeneous intralamellar shear, referred to below as the deck-of-cards mode. The top curve is for pearlite oriented parallel to the longitudinal axis and the others are for randomly oriented pearlite. All the curves asymptotically approach a limiting slope of $\frac{1}{4}$, the experimentally observed value, despite variations in initial orientation and deformation mode. Note especially that the deck-of-cards mode is exhausted and insignificant beyond relatively low strains. Note also that the rate of strain hardening is quite rapid during operation of the deck-of-cards mode. This form of strain-hardening curve has not been observed experimentally.

A second series of calculations was made, using the assumptions corresponding to various combinations of homogeneous plane strain elongation and deck-of-cards elongation; the results are shown in Fig. 11. The deck-of-cards deformation mode is the same as in Fig. 10, but the homogeneous deformation mode has been

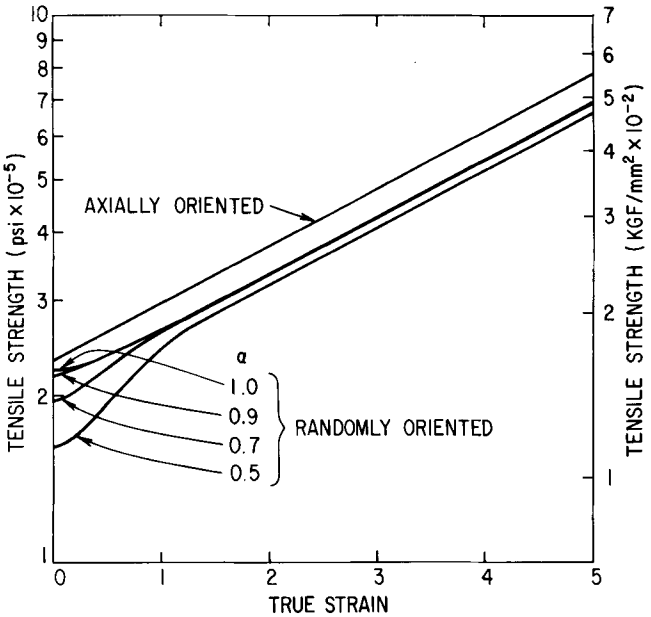

Fig. 10—Calculated flow stress-strain curves for initially axially aligned, and for randomly oriented pearlite, for various combinations of homogeneous axially symmetric and inhomogeneous deck-of-cards elongation.

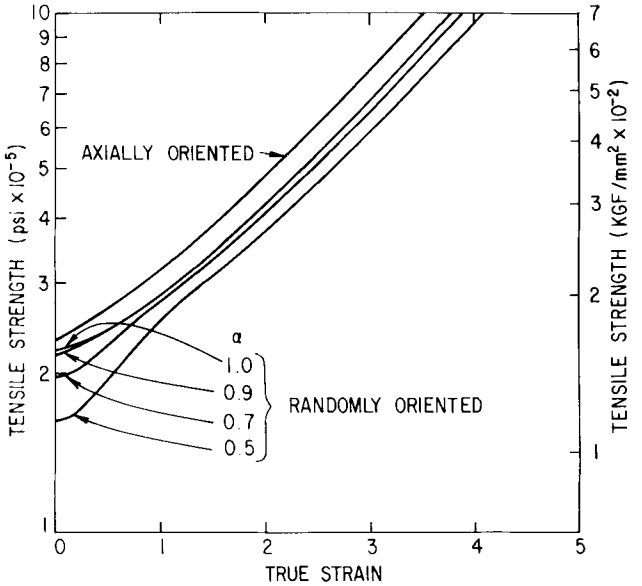

Fig. 11—Calculated flow stress-strain curves for initially axially aligned, and for randomly oriented pearlite, for various combinations of homogeneous plane strain and inhomogeneous deck-of-cards elongation.

changed from axially symmetric to plane strain elongation. The top curve is again for oriented pearlite, and the lower curves are for randomly oriented pearlite. All the curves asymptotically approach a limiting slope of $\frac{1}{2}$. This will be discussed below. The same comments about the deck-of-cards mode as made above apply here also.

There are several possibilities for the failure of the calculations summarized in Fig. 11 to predict the experimentally observed strengthening rate:

1) the ⟨110⟩ bcc wire texture was assumed perfect from the very beginning of the deformation, while experimentally a strain of about 0.5 is necessary to develop a detectable ⟨110⟩ texture, which continues to sharpen at higher strains. This error would have the effect of overestimating the strengthening rate, especially at low strains.

2) The initial strengthening rate is zero, especially for oriented pearlite and also for homogeneously deforming randomly oriented pearlite. Experimental scatter, or other more transient strain hardening mechanisms affecting the σ_0 term in Eq. [20], could hide this low initial rate and lower the overall strengthening rate, up to the highest strains yet investigated, $\epsilon \sim 4$.

3) If cementite lamellae were fragmented by deformation, the average strain in the cementite would be lower than the applied strain. The probability (p) of intersecting a given platelet would then be lowered from unity according to the equation,

$$p = \exp(\epsilon_{cm} - \epsilon) \qquad [21]$$

where ϵ and ϵ_{cm} are the applied and cementite strains respectively, thereby inversely raising the intercept interlamellar spacing above the projected interlamellar spacing and reducing the rate of strain hardening. This would alter the approximate equation for the change in $\bar{d}$ with strain, by homogeneous plane strain elongation, from

$$\bar{d} = \bar{d}_0 \exp(-\epsilon) \qquad [22]$$

to

$$d = \frac{\bar{d}_0}{p} \exp(-\epsilon) \qquad [23]$$

which, when combined with Eq. [21] becomes

$$\bar{d} = \bar{d}_0 \exp(-\epsilon_{cm}) \qquad [24]$$

A schematic representation of this process is shown in Fig. 12 for the case where ϵ_{cm} is one half of ϵ. Thus, a strain-hardening slope of $\frac{1}{4}$ would result for $\epsilon_{cm} = \frac{1}{2}\epsilon$ because Eq. [24] can then be combined with Eq. [20] to yield Eq. [1].

There are additional data in the literature which support this hypothesis: The transverse intercept spacing of rolled pearlite measured on transmission electron micrographs of edge sections by Embury *et al.*[13] decreases more slowly than in simple proportion to the strip thickness; analysis of their data indicates that the intercept spacing varies with strain according to the approximate equation,

$$\bar{d} = \bar{d}_0 \exp(-0.43\,\epsilon) \qquad [25]$$

If it can be assumed that this is entirely due to fragmentation of the cementite lamellae, rather than to some kind of inhomogeneous deformation, the strain in the cementite in this rolled pearlite is therefore 43 pct of the applied strain.

These possibilities will be discussed further with respect to their effects on the distribution of apparent interlamellar spacings.

Fig. 13 contains a series of families of histograms representing the changes in the distribution of apparent interlamellar spacings (transverse sections) with prior strain. The deformation modes are the same as those in Fig. 10. As it was assumed for simplicity in the calculations that there was but one initial spacing, there is no distribution or even the development of a distribution of spacings for axially symmetrically elongated, oriented pearlite. The microstructure of a transverse section simply remains similar to itself throughout the deformation.

The spacing distribution of homogeneously and axisymmetrically elongated pearlite remains unchanged, but the width of the spacing distribution is reduced by operation of the deck-of-cards deformation mode. Fig. 14 shows the distribution of axial ratios of the ribbon-like microregions resulting from this deformation mode as would be viewed on a transverse section for a series of increasing strains. Although these axial ratios are large enough to be potentially detectable, they are not large enough to account for the microstructures in Fig. 4. Also, the calculated lamellar traces in each of the ribbons are always aligned per-

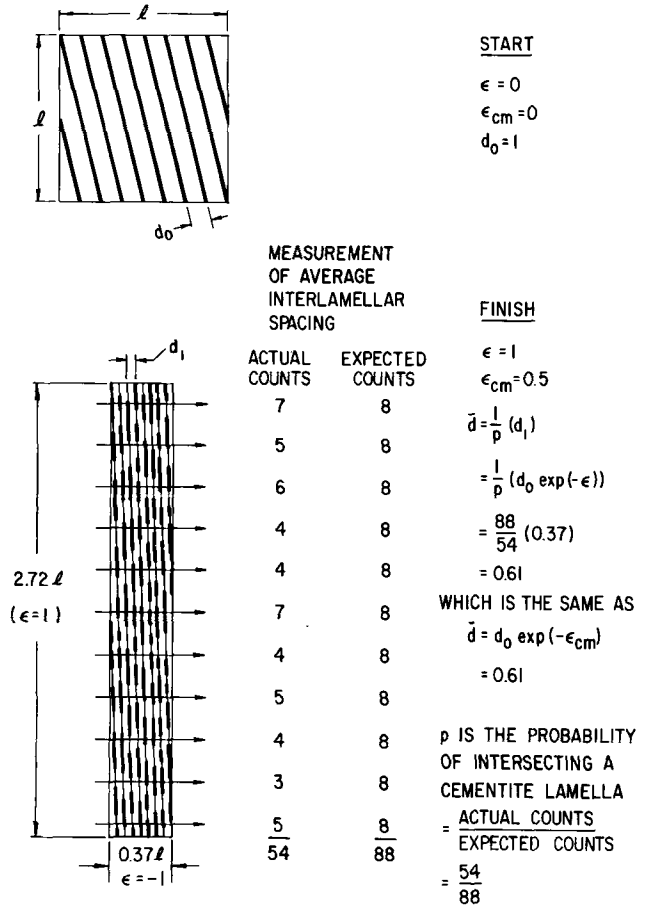

Fig. 12—Schematic representation of the effect of fragmentation of the cementite lamellae in a pearlite colony on the average interlamellar spacing as viewed on a longitudinal section.

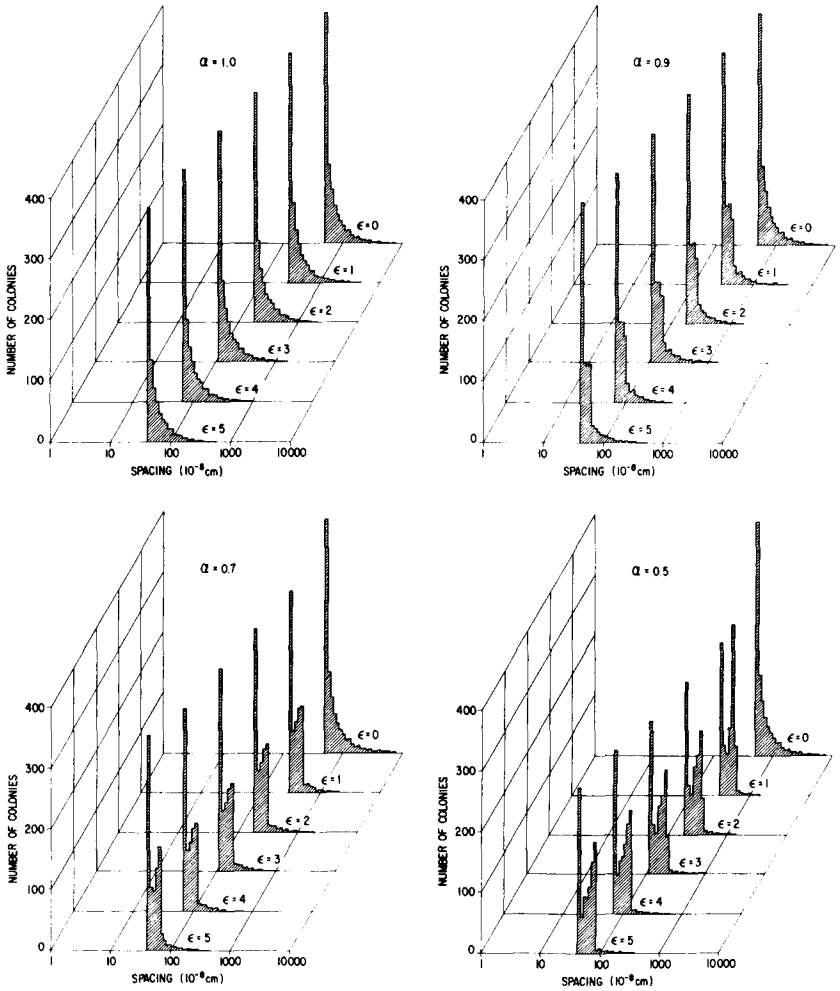

Fig. 13—Calculated apparent spacing distributions on transverse sections of drawn pearlitic wires as a function of strain by various combinations of homogeneous axially symmetric and inhomogeneous deck-of-cards elongation. Histograms are normalized to have equal areas.

pendicular to the thinnest dimension, as demanded by the deck-of-cards deformation mode, but contradictory to Fig. 5. Thus, the computed effects of the deck-of-cards deformation mode on the microstructure are incompatible with the experimental observations, so that it is unlikely that this is the dominant deformation mode or a significant cause of the "wavy" microstructure.

Fig. 15 shows two more families of histograms representing the changes in the spacing distribution for homogeneous plane strain elongation of randomly oriented pearlite and of axially aligned pearlite. Note that the widths of these distributions increase rapidly with increasing strain. For axially aligned pearlite, where the apparent spacings are also the true spacings, the ratio of the largest to the smallest spacing is $\exp(\epsilon)$. For a perfect $\langle 110 \rangle$ texture, the axial ratio of every ribbon should also be $\exp(\epsilon)$, so that at strains of 1, 2, 3, and 4 each ribbon would have an axial ratio of about 2.7, 7.4, 20, and 55, respectively. Unfortunately, the microstructures of the actual drawn, randomly oriented pearlite in Fig. 4 are too complicated and unresolved to allow comparable quantitative measurements. However, the degree of waviness and the axial ratios of at least a few pearlite colonies increase rapidly with strain, in qualitative agreement with the calculations.

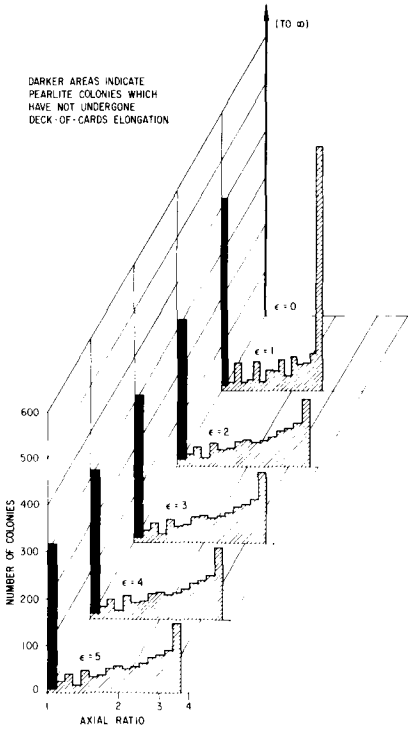

Fig. 14—Calculated axial ratio distributions of pearlite colonies on transverse sections of drawn wires as a function of strain when the critical resolved intralamellar shear strength is $\frac{1}{2}$ of the stress for homogeneous flow.

Fragmentation of the cementite would not alter the widths of the spacing distributions if it occurred without regard to orientation, but would reduce the rate of refinement of the structure. Hence, direct measurements of the distribution of spacings and the effect of strain on the average spacing of drawn pearlite would

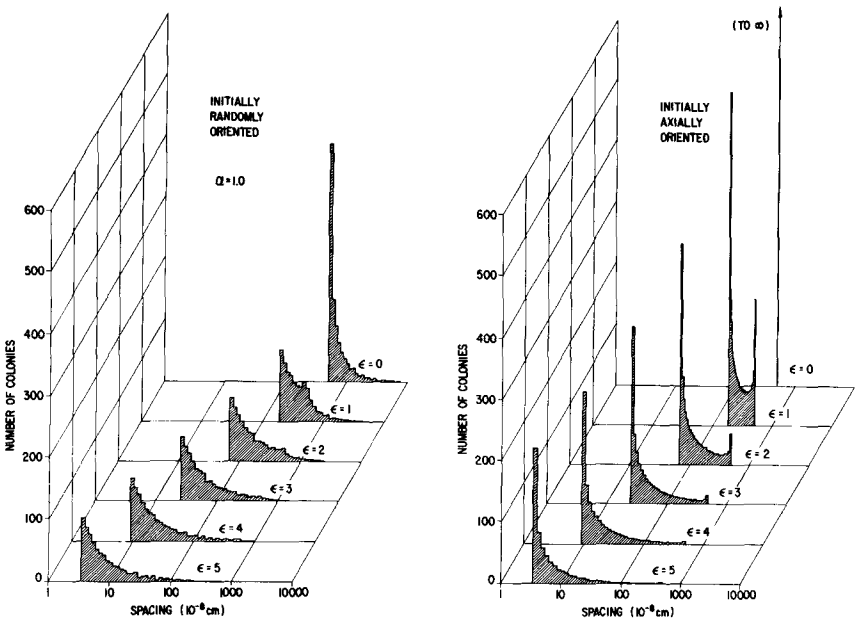

Fig. 15—Calculated apparent spacing distributions on transverse sections of drawn pearlitic wire as a function of strain by plane strain elongation. Both curves are normalized to have the same areas as in Fig. 13.

detect this effect as well as the effects of the ⟨110⟩ wire texture on the microstructure. The work would be much simplified if initially axially aligned pearlite were used.

The microstructural shape change in rolling is nearly the same as the external shape change, which is plane strain if there is no spreading. Since the state of stress is similar, *i.e.*, highly compressive, the rates of fragmentation of the cementite should be similar in wire drawing and in rolling, as was assumed in comparing Eqs. [24] and [25]. The strengthening mechanism is probably the same, so the rate of strain hardening ought to be the same in spite of the external differences in shape change of the specimens. This is so, as shown in Fig. 16, in which the tensile strengths of rolled fine pearlite are plotted as a function of true strain, $\ln(t_0/t)$, where t_0 and t are the original and instantaneous specimen thicknesses, respectively. These data were obtained by Grange[14] for the same set of specimens that Embury *et al.*[13] used to measure the change in transverse intercept spacings described by Eq. [25]. This provides additional evidence that the local shape change in drawn patented steel wire is plane strain elongation.

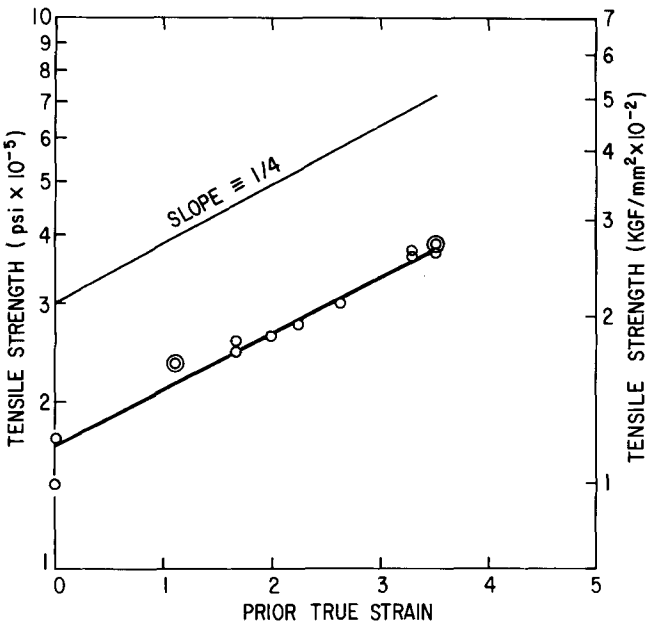

Fig. 16—Tensile strengths of the rolled fine pearlite used for the substructural spacing measurements of Embury *et al.*,[13] after Grange.[14]

No distinction need be made between the spacing of carbide particles in a transverse direction as used in this paper and the spacing between dislocation cell walls used by others[1,2] in similar structures, because the former spacing probably controls the latter; the dislocation cell walls probably possess higher mobility during the deformation than the carbide particles. Thus, in Fig. 12, the fine lines connecting the carbide particles need not represent cell walls but merely indicate the planes of the original unbroken lamellae.

In the future, during discussions of the strengthening mechanism in these materials as opposed to the mechanisms of deformation and local shape change which are emphasized in the present paper, such a distinction will need to be made. It is not now clear whether the Hall-Petch relation is followed in drawn steel wires because of the necessity of cutting the carbide particles with the aid of dislocation pileups in the ferrite, or because of a grain- or cell-size effect in the ferrite, or because of some other mechanism, such as the one proposed qualitatively by Chandhok *et al.*[2] The cutting of carbide particles by piled-up dislocations can account for the observed strengths of the drawn pearlite if the strength of the cementite is constant and on the order of 2×10^6 psi (1400 kgf per sq mm). The dislocations are too stiff to form closed loops within the very small dislocation cells in the drawn pearlite, in contrast to the mechanism proposed by Langford and Cohen[8,15] for the strengthening effect of the much larger cells in wire-drawn iron. This mechanism would bring about a direct relationship between strength and $(\bar{d})^{-1}$, and the constant of proportionality[8,15] is too high to be applied to the material used here.

CONCLUSIONS

When the cold drawn into wire, pearlite develops a "wavy" microstructure in transverse sections because of the ⟨110⟩ bcc wire texture of the ferrite. The paucity of slip systems in this texture causes the shape change of at least some of the interwoven ribbon-like microregions, corresponding approximately to the pearlite colonies, to be nearly plane strain elongation, insofar as can be determined from the experimental evidence presented here.

Calculation of the rate of strain hardening and the distribution of apparent interlamellar spacings by computer have shown that a model based on another possible mechanism of local plane strain elongation, inhomogeneous intralamellar shear, is not consistent with the microstructural evidence or the observed strain hardening rate.

Similar calculations have been made using a model corresponding to locally homogeneous plane strain elongation, as would be brought about by the ⟨110⟩ wire texture, in order to predict the spacing distributions of randomly oriented and also axially aligned pearlite for later quantitative comparison with more detailed measurements on electron micrographs of transverse sections of drawn pearlite, especially drawn initially axially aligned pearlite, which would be simpler to handle by the existing quantitative metallographic methods. It was found necessary to consider fragmentation of the cementite in the model in order to obtain the observed strain hardening rate and change of the average transverse intercept spacing with strain. Also, the *degree* to which the ⟨110⟩ bcc wire texture affects the microstructural shape changes has yet to be determined, as it is the average shape change of the entire microstructure which controls the strain hardening rate. Comparison of the strain hardening rates of wire-drawn pearlite and rolled pearlite suggest that the local microstructural shape change in both is indeed plane strain elongation.

Both the process of fragmentation of the cementite and the development of the ⟨110⟩ bcc wire texture can be expected to be somewhat sensitive to metallurgical structure and processing variables, such as die geometry, as well. This means that there may yet be the possibility of improving the strain-hardening rate of drawn pearlitic or bainitic structures in steel.

A simplified equation approximately describing the strain-hardening rate of drawn pearlite or bainite, according to the most likely model, is

$$\sigma = \sigma_0 + \frac{k_y}{\sqrt{\beta d_0}} \exp(\epsilon_{cm}/2) \qquad [26]$$

where β is between 1 and 2 and σ_0, ky, and ϵ_{cm} are as defined previously. This equation assumes 1) the Hall-Petch relation between flow strength and substructural scale and 2) locally homogeneous plane strain elongation within the wire.

Eq. [26] produces the same numerical result as the Embury-Fisher equation (Ref. 1, also Eq. [1] of this paper) but corrects their erroneous assumptions of homogeneous axially symmetric elongation and absence of dynamic recovery.

ACKNOWLEDGMENT

The author gratefully acknowledges the contributions and assistance of C. A. Johnson and R. C. Glenn of the E. C. Bain Laboratory for Fundamental Research and G. T. Spare and L. L. Longanecker of the Applied Research Laboratory.

REFERENCES

1. J. D. Embury and R. M. Fisher: *Acta Met.*, 1966, vol. 14, p. 147.
2. V. K. Chandhok, A. Kasak, and J. P. Hirth: *Trans. ASM*, 1966, vol. 59, p. 288.
3. M. A. P. Dewey and G. W. Briers: *J. Iron Steel Inst.*, 1966, vol. 204, p. 102.
4. R. C. Glenn, G. Langford, and A. S. Keh: *Trans. ASM*, 1969, vol. 62, p. 285.
5. J. F. Peck and D. A. Thomas: *Trans. TMS-AIME*, 1961, vol. 221, p. 1240.
6. E. S. Meieran and D. A. Thomas: *Trans. TMS-AIME*, 1965, vol. 233, p. 937.
7. W. F. Hosford, Jr.: *Trans. TMS-AIME*, 1964, vol. 230, p. 12.
8. G. Langford and M. Cohen: *Trans. ASM*, 1969, vol. 62, p. 623.
9. R. S. Cline, P. E. Toohill, and Hsun Hu: E. C. Bain Laboratory for Fundamental Research, U. S. Steel Corp., Monroeville, Pa., unpublished.
10. G. T. Spare and A. M. Mills: Applied Research Laboratory, U. S. Steel Corp., unpublished.
11. R. C. Glenn and R. D. Schoone: *Rev. Sci. Inst.*, 1964, vol. 34, p. 1223.
12. J. D. Embury and R. M. Fisher: E. C. Bain Laboratory for Fundamental Research, U. S. Steel Corp., Monroeville, Pa., unpublished.
13. J. D. Embury, A. S. Keh, and R. M. Fisher: *Trans. TMS-AIME*, 1966, vol. 236, p. 1252.
14. R. A. Grange: E. C. Bain Laboratory for Fundamental Research, U. S. Steel Corp., Monroeville, Pa., unpublished.
15. G. Langford and M. Cohen: to be submitted.